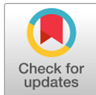

Research Article | Vol. 26, No. 7 | 2 Apr 2018 | OPTICS EXPRESS 8194

Optics EXPRESS

Wafer-scale nanopatterning using fast-reconfigurable and actively-stabilized two-beam fiber-optic interference lithography

CHUWEI LIANG,[1,2] TUO QU,[1,2] JINGXUAN CAI,[1] ZHOUYANG ZHU,[1] SHIJIE LI,[1] AND WEN-DI LI[1,*]

[1]*Department of Mechanical Engineering, the University of Hong Kong, Pokfulam, Hong Kong, China*
[2]*These authors contribute equally to this paper*
[*]*liwd@hku.hk*

Abstract: A fast-reconfigurable and actively-stabilized fiber-optic interference lithography system is demonstrated in this paper. Employment of fiber-optic components greatly enhances the flexibility of the whole system, simplifies its optical alignment, and suppresses the interference of mechanical vibrations. Active stabilization is implemented in the system and evaluated through modeling and experiment. We demonstrate 3-inch-diameter wafer-scale patterning of 240-nm-period grating lines with a sub-50-nm linewidth and an aspect ratio over 3. Two-dimensional patterns of different geometries and dimensions are also demonstrated to show the versatility of our system. Step-and-repeat exposure is demonstrated with independently controlled patterning fields of $2 \times 2\ cm^2$ large.

© 2018 Optical Society of America under the terms of the OSA Open Access Publishing Agreement

OCIS codes: (090.2880) Holographic interferometry; (060.2310) Fiber optics; (220.3740) Lithography; (220.4241) Nanostructure fabrication; (050.1950) Diffraction gratings.

References and links

1. H. I. Smith, "Low cost nanolithography with nanoaccuracy," Physica E **11**(2-3), 104–109 (2001).
2. P. T. Konkola, C. G. Chen, R. K. Heilmann, C. Joo, J. C. Montoya, C.-H. Chang, and M. L. Schattenburg, "Nanometer-level repeatable metrology using the Nanoruler," J. Vac. Sci. Technol. B **21**(6), 3097–3101 (2003).
3. J. Spallas, A. Hawryluk, and D. Kania, "Field emitter array mask patterning using laser interference lithography," J. Vac. Sci. Technol. B **13**(5), 1973–1978 (1995).
4. H. Liu, Y. H. Yao, Y. F. Wang, and W. Wu, "Full-color reflective display system based on high contrast gratings," J. Vac. Sci. Technol. B **32**, 4901416 (2014).
5. M. R. Gartia, Z. Xu, E. Behymer, H. Nguyen, J. A. Britten, C. Larson, R. Miles, M. Bora, A. S. P. Chang, T. C. Bond, and G. L. Liu, "Rigorous surface enhanced Raman spectral characterization of large-area high-uniformity silver-coated tapered silica nanopillar arrays," Nanotechnology **21**(39), 395701 (2010).
6. L. Zeng, P. Bermel, Y. Yi, B. Alamariu, K. Broderick, J. Liu, C. Hong, X. Duan, J. Joannopoulos, and L. Kimerling, "Demonstration of enhanced absorption in thin film Si solar cells with textured photonic crystal back reflector," Appl. Phys. Lett. **93**(22), 221105 (2008).
7. P. Wong, G. Balakrishnan, N. Nuntawong, J. Tatebayashi, and D. Huffaker, "Controlled InAs quantum dot nucleation on faceted nanopatterned pyramids," Appl. Phys. Lett. **90**(18), 183103 (2007).
8. S. O. Kim, H. H. Solak, M. P. Stoykovich, N. J. Ferrier, J. J. De Pablo, and P. F. Nealey, "Epitaxial self-assembly of block copolymers on lithographically defined nanopatterned substrates," Nature **424**(6947), 411–414 (2003).
9. L. J. Guo, "Nanoimprint lithography: methods and material requirements," Adv. Mater. **19**(4), 495–513 (2007).
10. W. Wu, B. Cui, X. Y. Sun, W. Zhang, L. Zhuang, L. S. Kong, and S. Y. Chou, "Large area high density quantized magnetic disks fabricated using nanoimprint lithography," J. Vac. Sci. Technol. B **16**(6), 3825–3829 (1998).
11. X. Chen, Z. Ren, Y. Shimizu, Y. L. Chen, and W. Gao, "Optimal polarization modulation for orthogonal two-axis Lloyd's mirror interference lithography," Opt. Express **25**(19), 22237–22252 (2017).
12. E. C. Chang, Y. L. Sun, P. T. Lin, D. G. Mikolas, and C. C. Fu, "Lloyd's Mirror Interference Lithography Using a Single Mode Fiber Spatial Filter," IEEE Sens. J. **2012**, 1416–1419 (2012).
13. Y. L. Sun, D. Mikolas, E. C. Chang, P. T. Lin, and C. C. Fu, "Lloyd's mirror interferometer using a single-mode fiber spatial filter," J. Vac. Sci. Technol. B **31**, 4790660 (2013).
14. Y. J. Hung, P. C. Chang, Y. N. Lin, and J. J. Lin, "Compact mirror-tunable laser interference system for wafer-scale patterning of grating structures with flexible periodicity," J. Vac. Sci. Technol. B **34**, 4955172 (2016).
15. J. He, X. Fang, Y. Lin, and X. Zhang, "Polarization control in flexible interference lithography for nano-patterning of different photonic structures with optimized contrast," Opt. Express **23**(9), 11518–11525 (2015).

#319883 https://doi.org/10.1364/OE.26.008194
Journal © 2018 Received 16 Jan 2018; accepted 15 Mar 2018; published 21 Mar 2018

16. J. Xu, Z. B. Wang, Z. K. Weng, Z. M. Li, X. J. Sun, L. J. Liu, L. Zhao, Y. Yue, and J. Zhang, "Laser Interference Nanolithography with a 405nm Fiber Semiconductor Laser," Key Eng. Mater. **552**, 262–267 (2013).
17. G. B. Hocker, "Fiber-optic sensing of pressure and temperature," Appl. Opt. **18**(9), 1445–1448 (1979).
18. L. S. Schuetz, J. H. Cole, J. Jarzynski, N. Lagakos, and J. A. Bucaro, "Dynamic Thermal Response of Single-Mode Optical Fiber for Interferometric Sensors," Appl. Opt. **22**(3), 478–483 (1983).

1. Introduction

Interference lithography (IL) is a widely adopted method to create dense, periodic nanoscale patterns without masks. Periodic nanopatterns created by IL can be further transferred to semiconductor substrates or other functional materials for device applications [1,2]. Through this process, IL has demonstrated promising and versatile applications in the fabrication of display panels [3, 4], surface-enhanced Raman sensing substrates [5], solar cells [6], and magnetic storage devices [7], just to name a few. Guided by IL-patterned structures, self-assembly of nanomaterials can achieve a much improved long-range order [8]. Particularly, IL has been used to fabricate master molds for nanoimprint lithography to fully unleash its potential in large-area, high-throughput nanomanufacturing [9, 10].

IL has been developed in various configurations. Lloyd's mirror type IL [11–13] is the most adopted configuration, where half of the wavefront of the beam is reflected by a mirror to overlap with the other half on the photoresist to form interference fringes. However, the patterning area in this configuration is typically a few cm^2 large, which is mainly limited by the mirror size and the beam intensity profile. Wafer-scale patterning mostly uses amplitude-division configurations, in which coherent sub-beams are generated using beam splitters and overlap to form interference patterns in photoresist. However, since the sub-beams travel in different paths, random variation in their relative phase difference caused by environmental disturbance may lead to interference pattern drifting that deteriorates the pattern contrast.

Most IL systems with amplitude-division configurations use free-space optics with precise alignment. Although multi-beam amplitude-division IL has demonstrated high-quality patterning over wafer-scale area [14], its free-space optics makes its setup, alignment, adjustment, and stabilization very challenging and usually can only be established by highly-skilled experts. Fiber-optic components have been used to replace free-space optics for reduced operation complexity and improved compactness of the system [15, 16]. However, employing fiber-optic delivery of coherent light in amplitude-division multi-beam IL systems is still challenging, because light propagation in optical fiber experiences randomly varying phase delay due to temperature variation, which adversely affects the pattern contrast [17, 18].

In this paper, we demonstrate large-area patterning using fast-reconfigurable and actively-stabilized amplitude-division fiber-optic interference lithography (FOIL) setup. Pattern drifting caused by temperature-sensitive phase delay variation and its stabilization using close-loop feedback are investigated using experiments and modeling. As demonstrations, we patterned versatile one-dimensional and two-dimensional structures over wafer-scale area, including 240-nm-period lines with a linewidth of 40 nm and an aspect ratio over 3, and pillars and holes of various dimensions and geometries. By employing an automatic sample stage, we also achieved step-and-repeat exposure over scalable, large area with 2-cm-by-2-cm exposure fields that can be independently controlled. These results show strong potential of multi-beam FOIL systems in high-quality, large-area nanopatterning.

2. Two-beam Fiber-optic Interference Lithography (2-FOIL) Setup

The schematic the 2-FOIL system is shown in Fig. 1(a). A single-mode single-frequency 405-nm diode laser (Ondax Inc., USA) is coupled to a customized polarization-maintaining fiber splitter through collimating optics. The laser beam is split into two coherent sub-beams, which emit out of two single-mode optical fiber cables connected to the splitter. The fiber output ports are mounted on two rotatable optical rails, so that the angle between the two sub-beams can be adjusted by rotating the rails while the distance from the output ports to the

Research Article Vol. 26, No. 7 | 2 Apr 2018 | OPTICS EXPRESS 8196
Optics EXPRESS

sample is fixed. At the junction of the two optical rails, a vacuum sample holder is mounted vertically to fix the samples during exposure. The sub-beams emit from the fiber ports, expand in free space, and then overlap on the sample stage to form the interference patterns. A photo of one actual 2-FOIL setup is shown in Fig. 1(b), with the light beams visualized using delayed photography with a moving screen, and Fig. 1(c) shows a photo of 440-nm-period grating patterned in the photoresist on a 3-inch fused silica wafer using this 2-FOIL setup.

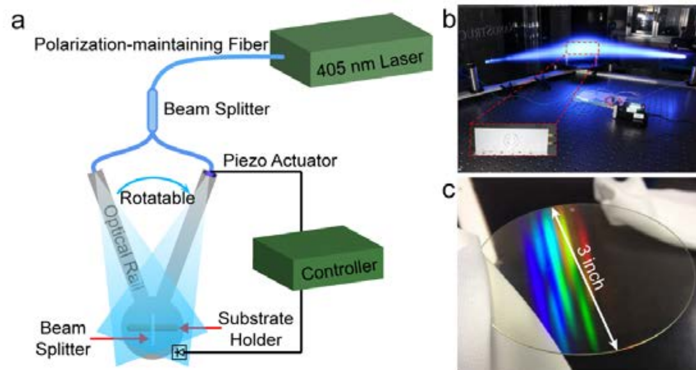

Fig. 1. Two-beam fiber-optic interference lithography setup. (a) System schematic. (b) Photograph of an actual setup with a homemade vacuum chuck (red box). (c) Photograph of a 3-inch fused silica wafer carrying 440-nm-period gratings patterned by the setup shown in (b).

This fiber-optic configuration offers a series of benefits by taking advantage of the flexibility of optical fiber. Particularly, the customized single-mode optical fiber and fiber-optic splitter replace free-space optical components that need to be strictly aligned and adjusted. Periodicity of interference patterns now can be easily tuned by rotating the optical rails holding the fiber ports. Single-mode fiber used here outputs an ideal circular Gaussian intensity profile for the exposure. Flexibility of fiber-optic components also helps to suppress the interference of high-frequency mechanical noise in the laboratory environment.

On the other hand, fiber-optic components in the 2-FOIL also introduce new challenges. Thermal fluctuations will cause the phases of the sub-beams to change when passing through the optical fiber due to thermal expansion and the temperature dependence of the refractive index of silica [17]. The overall temperature dependence of the phase delay is calculated to be $245\, rad / \left({}^{\circ}C \cdot m\right)$. Since the phases in the sub-beams vary independently and randomly, the interference fringes will exhibit random drifting that deteriorates the pattern contrast. An active stabilization mechanism needs to be implemented to improve the patterning quality.

3. Enhanced Pattern Contrast by Active Stabilization

Active stabilization of the 2-FOIL system is realized through directly moving one fiber output port using a piezo-actuated stage to compensate the random variation of the phase difference between the two beams. The phase difference variation is detected using an interferometry setup that comprises a plate beam splitter located under the center of the sample holder, and a photodetector placed behind the beam splitter. When the two beams are combined at the beam splitter, the variation of the phase difference between them is converted into light intensity variation and detected by the photodetector. The output of the photodetector is used as the input of a proportional-integral-derivative (PID) control algorithm to generate the high-voltage actuation signal for the piezo-actuator. The random variation of the phase difference is a low-frequency signal because it is mainly caused by thermal fluctuation along the fiber. Sampling and actuation in our active stabilization system are performed at a rate of 1000 Hz.

Optics EXPRESS

The light intensity signal detected by interferometry can be used to estimate the contrast of the interference patterns on the exposed photoresist. The intensity profile of the interference pattern on the photoresist is calculated as Eq. (1),

$$I(x,t) = 2I_0\left\{1+\cos\left[\frac{4\pi}{\lambda}\sin\theta\cdot x+\Delta\varphi(t)\right]\right\} \tag{1}$$

where λ is the laser wavelength, θ is the half angle between the two sub-beams, I_0 is the intensity of the beams incident on the photoresist (assuming the two beams have equal intensities), x is the horizontal distance from the center of the exposure spot, and $\Delta\varphi(t)$ is the relative phase difference between the two sub-beams, which is randomly varying due to the thermal fluctuation. $\Delta\varphi(t)$ can be extracted using the light intensity measured at the interferometry detection point if a fixed phase offset is ignored. The light intensity detected by the interferometry setup can be normalized with its maximum value and is related to the variation of the phase difference between the two beams according to $I_1'(t)=\frac{1}{2}\left[1+\cos\Delta\varphi(t)\right]$, where $I_1'(t)$ is the normalized interferometry output. Therefore, $\Delta\varphi(t)$ can be derived as $\Delta\varphi(t)=\arccos\left[2\times I_P'(t)-1\right]$. Typical variations of phase difference between the two beams are shown in Figs. 2(a) and 2(c), when the active stabilization was off and on, respectively. The results were recorded for 60 s, which is comparable to the typical exposure time. Their corresponding occurrence frequency distributions are plotted in Figs. 2(b) and 2(d). Obviously, when the active stabilization was on, the two sub-beams had nearly constant phase difference, corresponding to stable patterns in the photoresist. However, when the active stabilization was off, the phase difference had a random distribution that led to drifting patterns.

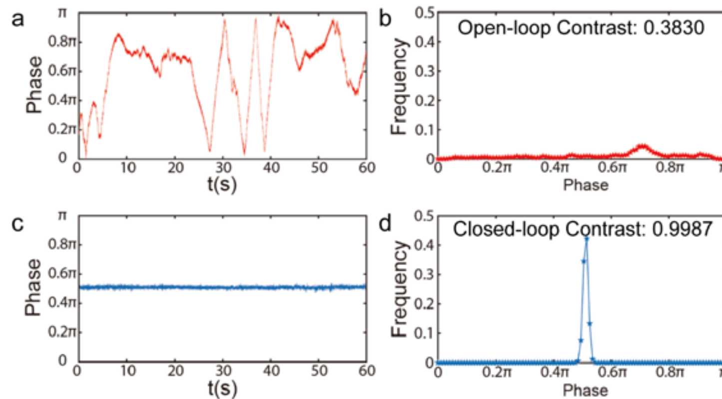

Fig. 2. Variation of the phase difference between the two sub-beams. (a) The varying phase difference and (b) its occurrence frequency for open-loop operation without active stabilization. (c) The varying phase difference and (d) its occurrence frequency for closed-loop operation with active stabilization. Calculated pattern contrasts are labeled in (b) and (d).

We can further estimate the pattern contrast using the measured phase difference variation, according to Eq. (2):

Optics EXPRESS

$$\text{Contrast} = \frac{\text{MAX}\left[\int_0^T I(x,t)\,dt\right] - \text{MIN}\left[\int_o^T I(x,t)\,dt\right]}{\text{MAX}\left[\int_0^T I(x,t)\,dt\right] + \text{MIN}\left[\int_o^T I(x,t)\,dt\right]} \tag{2}$$

where T is the total exposure time, I(x,t) is calculated using Eq. (1) with the extracted relative phase difference $\Delta\varphi(t)$, and the maxima and minima values are obtained within one period of the fringe. The pattern contrasts of the exposure without (Figs. 2(a) and 2(b)) and with (Figs. 2(c) and 2(d)) active stabilization are therefore estimated to be 0.3830 and 0.9987, respectively.

In Fig. 3(a), we show intensity profiles of interference grating patterns simulated using Eq. (1) according to experimentally recorded phase differences. Simulated intensity pattern A with the active stabilization, which had a calculated pattern contrast of 0.9877, clearly shows better quality than pattern A', which was exposed without the stabilization and had a contrast of 0.1622. Figure 3(b) compares the corresponding actual exposed interference pattern quality. Silicon substrates with spincoated AZ1500 photoresist (Clariant, Switzerland) were used in the exposure. Atomic force microscopy (AFM) characterization shows that sample A, which was exposed with active stabilization, shows sharper grating patterns than sample A' that had no stabilization during exposure, which is consistent with the simulation results in Fig. 3(a). Using the actively stabilized 2-FOIL system, we successfully fabricated 240-nm-period gratings with a 40-nm linewidth and a 130-nm height, corresponding to an aspect ratio of 3.25, as shown in Fig. 3(c).

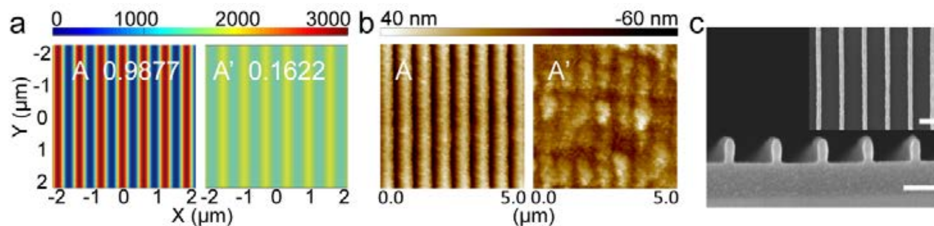

Fig. 3. (a) The simulated intensity patterns with (A) and without (A') active stabilization. The simulation was based on recorded phase difference variation. (b) The AFM images of the actual grating patterns corresponding to simulated patterns in (a). (c) SEM images of 240-nm-period, 40-nm-linewidth grating. The scale bars are 200 nm.

4. Large-area Patterning of Periodic Nanostructures

The large-area fabrication capability of the stabilized 2-FOIL system is demonstrated by patterning various periodic nanostructures on 3-inch-diameter wafers. SEM images in Fig. 4(a) were taken on 240-nm-period grating structures on different positions on a 3-inch silicon wafer, exhibiting less than 15% variation of grating linewidth over the whole sample. The increasing linewidth from the center to the edge is caused by the Gaussian distribution of the laser spots exposing on a positive-tone photoresist. In our 2-FOIL system, laser beams emitted from the fiber ports are naturally expanded in free space to cover the whole wafer. Our patterning area is mainly limited by the available lab space, which only allows a beam expansion length of approximately 1 m. With a longer beam expansion length, our system can be used for patterning on larger wafers. The system can be extended to produce two-dimensional patterns by exposing the sample more than one time with a rotation angle. As examples, Figs. 4(b) and 4(c) show the SEM images of a dot array and a hole array in the exposed photoresist through double exposure with 90° and 10° rotation angles, respectively.

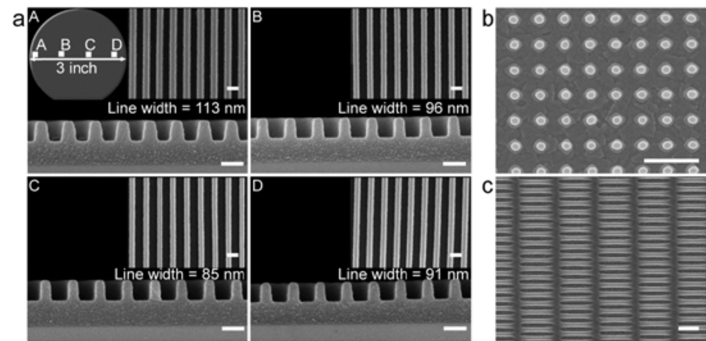

Fig. 4. Large-area patterning of periodic nanostructures on 3-inch wafers. (a) SEM images on 4 different locations across a 3-inch wafer with 240-nm-pitch gratings show good uniformity of grating linewidth. Scale bars in (a) are 200 nm. (b) Two-dimensional dot array and (c) hole array fabricated using 2-FOIL setup on 3-inch wafers. Scale bars in (b) and (c) are 1 μm .

To achieve large-area patterning using our 2-FOIL setup, a step-and-repeat exposure configuration is also adopted. A 2-cm-by-2-cm square aperture is placed in front of the wafer and a timer-controlled shutter covers the opening aperture to set the exposure time. The wafer is placed on a motorized stage. The two laser beams pass through the square aperture and interfere on the sample within the 2-cm-by-2-cm square patterning area when the shutter is open. The motorized stage moves the wafer so that multiple 2-cm-by-2-cm square patterns can be exposed consequently to cover the whole sample. The motorized stage can also rotate the sample to enable patterning of two-dimensional dots and holes. Since our 2-FOIL system is fast-reconfigurable, each patterning area can be independently controlled with set pattern periodicity, exposure time, and pattern shape. Figure 5 shows a 3-inch wafer exposed with 9 patterning fields of two-dimensional pillar arrays of hexagonal lattice with various periods of 500 nm, 900 nm, and 700 nm, and different exposure times, respectively.

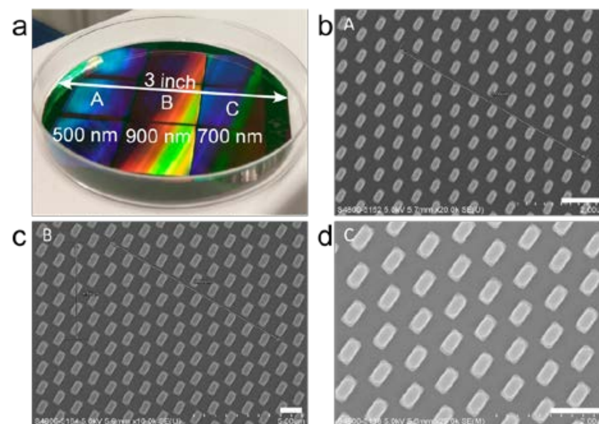

Fig. 5. Step-and-repeat exposure. (a) Photograph of a 3-inch silicon wafer with pillar arrays of hexagonal lattice (Period: left column: 500 nm, middle column: 900 nm, right column: 700 nm) patterned by the step-and-repeat exposure configuration. (b)(c)(d) The SEM images from a top view of position A, B, and C. The scale bars are 1 μm .

5. Conclusion

In this paper, we introduce a 2-FOIL system with fast reconfigurability and active pattern stabilization. The system is compact, stable, and versatile, due to the use of fiber-optic components for light delivery and laser beam shaping. An interference fringe stabilization technique that comprises a piezoelectric actuator and an interferometry setup is implemented

to achieve high contrast in the exposed patterns. Wafer-scale patterning of 240-nm-period gratings with an aspect ratio up to 3.25 demonstrates the high patterning quality of our 2-FOIL system. Step-and-repeat exposure is also developed for our 2-FOIL system for wafer-scale patterning with individually controlled patterning fields of $2\times2\ cm^2$ size.

Funding

Research Grants Council of Hong Kong (HKRGC) (27205515 and 17246116); Science and Technology Innovation Commission of Shenzhen Municipality (JCYJ20140903112959959); Department of Science and Technology of Zhejiang Province (2017C01058).

147.8.230.39 {ts '2018-11-13 22:12:52'}